J. Fluid Mech. (1995), *vol.* 287, *pp.* 199–223

Effect of wire separation on X-probe measurements in a turbulent flow

By Y. ZHU AND R. A. ANTONIA

Department of Mechanical Engineering, University of Newcastle, N.S.W., 2308, Australia

(Received 16 July 1993 and in revised form 16 August 1994)

The effect of the separation between hot wires in a crossed wire or X-probe on Reynolds stress measurements has been studied analytically and experimentally. Wyngaard's (1968) spectral analysis, which assumes isotropic turbulence, has been modified to include the effect of the tangential velocity component and possible asymmetries of the probe. The relaxation of the assumption of isotropy to one of homogeneity allows corrections to be made to Reynolds stress measurements obtained when the separation between the wires is in the spanwise direction. Measurements with two inclined hot wires in the central region of a fully developed turbulent channel flow provide reasonable support for the modified analysis. In the anisotropic wall region, the measurements provide reasonable support for the correction ratios which have been derived by assuming that turbulence is homogeneous in a plane parallel to the wall.

1. Introduction

Crossed wires or X-probes are commonly used for measuring two components of the fluctuating velocity vector in turbulent flows. The accuracy of the measurement depends, in general, on the following factors (e.g. Vukoslavčević & Wallace 1981; Perry 1982; Nakayama & Westphal 1986; Browne, Antonia & Shah 1988; Antonia 1991; Park & Wallace, 1992; Tagawa, Tsuji & Nagano 1992)

(*a*) rectification or the insensitivity of the hot wires to the direction of the instantaneous velocity vector in a turbulent flow;

(*b*) influence of the tangential (along the length of each wire) and binormal velocity components (normal to the plane of the wires);

(*c*) probe geometry, such as wire length, wire diameter, the separation between the two wires and the effective angles of the two wires.

The errors due to rectification and the influence of the binormal velocity component have been studied by several authors (e.g. Bruun 1972; Tutu & Chevray 1975; Kawall, Shokr & Keffer 1983; Swaminathan, Rankin & Sridhar 1986; Tagawa *et al.* 1992). The effect of geometry, especially the separation between the wires, on measured turbulence statistics has also been investigated, e.g. Wyngaard 1968; Bremhorst 1972; Nakayama & Westphal 1986; Westphal 1990; Suzuki & Kasagi 1990; Tagawa *et al.* 1992. Wyngaard (1968) proposed a correction method for the lengths of the hot wires and for their separation. Isotropic turbulence and a first-order approximation for the X-probe response equations were assumed. The cooling effect of the tangential and binormal velocity components was neglected. Also, the X-probe was assumed to be symmetrical about the streamwise flow axis x. Bremhorst's (1972) proposal for correcting the measured Reynolds stresses and their spectra requires a knowledge

of two-point velocity correlations within the volume occupied by the X-probe. Such data have only recently become available through direct numerical simulations (DNS). Westphal (1990) used Wyngaard's response equations and derived correction ratios for the Reynolds stresses by assuming a simplified (homogeneous) form of two-point velocity correlations. Suzuki & Kasagi (1990) included the tangential velocity component in the response equations and used DNS correlation data (Kuroda, 1990) for evaluating correction ratios.

In the analyses of Bremhorst, Westphal and Suzuki & Kasagi, isotropy was not assumed but the effect of the binormal velocity component was neglected, and a symmetrical configuration of the X-probe was used. Browne *et al.* (1988) investigated the effect of separation on the measured Reynolds stresses in the self-preserving wake of a circular cylinder. The effect on $\overline{u^2}$ and $\overline{v^2}$ was in qualitative agreement with that predicted from the analyses of Westphal (1990) and Suzuki & Kasagi (1990). However, the experiment was confined to the use of only one particular X-probe configuration (approximately symmetrical wires at $\pm 45°$ to the x axis) and one measurement location where the departure from isotropy was small (Antonia, Browne & Shah 1988*a*; Antonia, Shah & Browne 1988*b*). Moreover, Browne *et al.* noted that the one-dimensional spectral response curves obtained using Wyngaard's analysis indicated trends for the Reynolds normal stresses which were opposite to those of the measurements, apparently implying that the analysis is not suitable for correcting X-probe data for the effect of wire separation. This inadequacy cannot be due to the inappropriateness of the isotropy assumption since Wyngaard's analysis for the effect of the separation between parallel hot wires on the measurement of velocity derivatives has received good experimental support in flow regions where local isotropy (or isotropy of the small scales) is satisfied approximately (Zhu & Antonia 1992, 1993; Zhu, Antonia & Kim 1993; Antonia, Zhu & Kim 1993). One would therefore expect it to be associated with the other assumptions (first-order response equations, perfect symmetry). One aim of the present paper is to assess the impact these assumptions have on Wyngaard's analysis for X-probes. Another aim is to relax the assumption of isotropy in order to provide a means of correcting X-probe data in flow regions where the departure from isotropy is significant.

Wyngaard's analysis is first modified by taking into account the cooling due to the tangential velocity component and the effect of possible asymmetries in the X-probe configuration, although high order terms in the cooling equations are neglected. Correction ratios for the Reynolds stresses are then derived using an empirical procedure which allows measurements of the Reynolds stresses to be corrected in flow regions which do not satisfy isotropy but which are approximately homogeneous in a plane parallel to the wall. The results from the analyses are compared with measurements in a fully developed turbulent channel flow. This flow was chosen partly because the Reynolds shear stress can be estimated with relatively good accuracy from measurements of the streamwise pressure gradient and partly because there are several DNS data bases which are available for this flow. The X-probe Reynolds stress data are also compared with those from other types of measurements, such as LDV (laser Doppler velocimetry) and PIV (particle image velocimetry).

2. Experimental details

Measurements were made in a fully developed turbulent channel flow (a definition sketch is shown in figure 1a) at a Reynolds number of 3300 ($Re = U_0 h/\nu$, where h

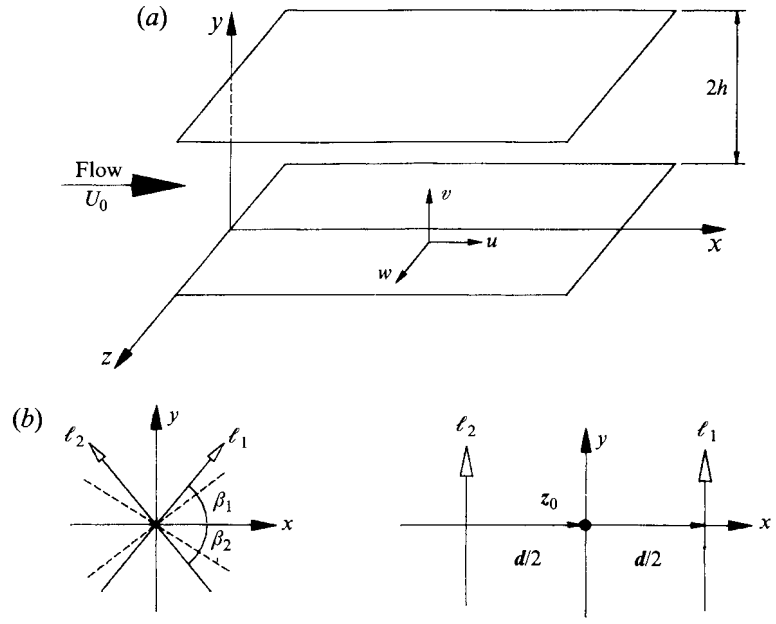

FIGURE 1. Definition sketch: fully developed channel flow (*a*) and X-probe configuration (*b*).

is the channel half-width, U_0 is the velocity at the centreline and ν is the kinematic viscosity), which is comparable to the values used in simulations and measurements (with LDV and PIV techniques). The working section of the duct is 7.32 m long, 0.76 m high and 0.042 m wide (aspect ratio = 18). The measurement location x/h (x is measured from the entrance to the working section) is 330. At this location, the flow is fully developed (e.g. Shah 1988). The channel aspect ratio is sufficiently large to ensure two-dimensionality of the mean flow (Teitel & Antonia 1990).

A single hot wire was used to measure the streamwise mean velocity and velocity fluctuation. For the measurement of the lateral velocity component, two inclined hot wires were arranged to form an X-probe. One of the wires was mounted on a traversing mechanism, while the other one was mounted on a separate (smaller) traversing mechanism (built in-house) which is fixed to the first traversing mechanism (Mitutoyo). In this way, the two wires could be moved as part of a single (fixed separation) probe to any location in the flow. Both traversing mechanisms have a least count of 0.01 mm. The spacing between the wires could be accurately varied using the smaller traversing mechanism and the initial spacing was measured by a theodolite (uncertainty ± 0.01 mm). The initial distance between the X-probe and the wall was measured using a theodolite and a reflection method.

The 2.5 μm diameter Wollaston Pt-10% Rh wires were used for all the probes. The wires were etched to an active length of 0.45–0.5 mm, and wires were operated at an overheat ratio of 1.5 with in-house constant temperature circuits. DC offset voltages were applied to the signals from these circuits before amplification and low-pass filtering at a cut-off frequency of 1000–1600 Hz. The signals were then digitized on an IBM-compatible PC using a 12 bit A/D converter at a sampling frequency 2–3 times greater than the filter frequency and subsequently transferred, via an ETHERNET optical link, to a VAX 780 computer for further analysis.

Velocity and yaw calibrations of the X-probe were carried out at the centre of the channel. The wires were in the (x, y)-plane and separated in the z-direction. A Pitot tube, connected to a Furness pressure transducer, was located on the channel centreline. The transducer output and the outputs from the wires were digitized at a sampling frequency of 100 Hz/channel.

3. Theoretical analysis for isotropic turbulence

The configuration of the X-probe is shown in figure 1(*b*). β_i $(i = 1, 2)$ is the effective angle between the wire axis and the streamwise direction. For convenience, the following assumptions are made :

(i) the wires lie exactly in the (x, y)-plane;

(ii) the sensitivity of each wire is uniform over the length of the wire;

(iii) the flow is homogeneous in the (x, z)-plane, which is parallel to the wall (normal to the plane of the X-probe);

(iv) the mean velocities in the wall-normal and spanwise directions are much smaller than the mean velocity in the streamwise direction, i.e. $\overline{V}/\overline{U} \ll 1$, $\overline{W}/\overline{U} \ll 1$;

(v) Jörgensen's (1971) equation for the effective cooling velocity is valid, i.e.

$$U_{ei}^2 = U_{Ni}^2 + k_{w_i}^2 U_{T_i}^2 + h_{w_i}^2 U_{B_i}^2 \quad , \tag{3.1}$$

where the subscript i denotes the wire number $(i = 1, 2)$, U_e stands for the effective cooling velocity; U_N, U_T and U_B are the normal, tangential and binormal velocity components respectively; k_w and h_w are the yaw and pitch factors.

Owing to assumption (iv), the three components of the velocity vector for the ith wire are $\tilde{U}_i = \overline{U}_i + u_i$, $\tilde{V}_i = v_i$, $\tilde{W}_i = w_i$. Equation (3.1) can be re-written as

$$U_{e_1}^2 = [(\overline{U}_1 + u_1)\sin\beta_1 - v_1\cos\beta_1]^2 + k_{w_1}^2[(\overline{U}_1 + u_1)\cos\beta_1 + v_1\sin\beta_1]^2 + h_{w_1}^2 w_1^2 \quad , \tag{3.2}$$

$$U_{e_2}^2 = [(\overline{U}_2 + u_2)\sin\beta_2 + v_2\cos\beta_2]^2 + k_{w_2}^2[(\overline{U}_2 + u_2)\cos\beta_2 - v_2\sin\beta_2]^2 + h_{w_2}^2 w_2^2 \quad . \tag{3.3}$$

for wires 1 and 2 respectively. Using the binomial theorem, (3.2) and (3.3) can be expressed as

$$U_{e_1} = \overline{U}_1(\sin^2\beta_1 + k_{w_1}^2\cos^2\beta_1)^{1/2}\left[1 + \frac{u_1}{\overline{U}_1} - \frac{(1 - k_{w_1}^2)\cot\beta_1}{1 + k_{w_1}^2\cot^2\beta_1}\frac{v_1}{\overline{U}_1} + R_1\right] \tag{3.4}$$

$$U_{e_2} = \overline{U}_2(\sin^2\beta_2 + k_{w_2}^2\cos^2\beta_2)^{1/2}\left[1 + \frac{u_2}{\overline{U}_2} + \frac{(1 - k_{w_2}^2)\cot\beta_2}{1 + k_{w_2}^2\cot^2\beta_2}\frac{v_2}{\overline{U}_2} + R_2\right] \quad , \tag{3.5}$$

where R_1 and R_2 represent higher-order terms. Since R_1 and R_2 are normally small, their contributions to the total cooling effect can be neglected. For example, for a fully developed turbulent channel flow at $Re = 3300$ (Kim, Moin & Moser 1987), the maximum turbulence levels are $u'/U = 0.35$; $v'/U = 0.07$ and $w'/U = 0.08$ respectively (hereafter, the prime denotes the root-mean-square value of the velocity fluctuation). The cooling effect due to the higher order term amounts to only 3–5% and can be neglected. From (3.4) and (3.5), the fluctuating effective velocities are

$$u_{e_1} = K_{u_1}u_1 - K_{v_1}v_1 \tag{3.6}$$

$$u_{e_2} = K_{u_2}u_2 + K_{v_2}v_2 \quad , \tag{3.7}$$

where

$$K_{u_i} = (\sin^2 \beta_i + k_{w_i}^2 \cos^2 \beta_i)^{1/2} \quad ,$$

and

$$K_{v_i} = (1 - k_{w_i}^2) \frac{\sin \beta_i \cos \beta_i}{K_{u_i}} \qquad (i = 1, 2) \quad . \tag{3.8}$$

The measured velocity fluctuations u^m and v^m, which are obtained by neglecting line averaging and the separation, are related to the true velocity fluctuations u_i, v_i (for the ith wire) by the following relations (e.g. Bremhorst 1972; Suzuki & Kasagi 1990)

$$K_{u_1} u^m - K_{v_1} v^m = K_{u_1} u_1 - K_{v_1} v_1 \quad , \tag{3.9}$$

$$K_{u_2} u^m + K_{v_2} v^m = K_{u_2} u_2 + K_{v_2} v_2 \quad . \tag{3.10}$$

The introduction of $K_1 = K_{v_1}/K_{u_1}$ and $K_2 = K_{v_2}/K_{u_2}$ allows K_1 and K_2 to be expressed in a more general form, viz.

$$K_i = (1 - k_{w_i}^2) \frac{\tan \beta_i}{k_{w_i}^2 + \tan^2 \beta_i} \quad . \tag{3.11}$$

After solving (3.9) and (3.10) for u^m and v^m, we obtain

$$u^m = \frac{K_2 u_1 + K_1 u_2}{K_1 + K_2} + K_1 K_2 \frac{v_2 - v_1}{K_1 + K_2} \tag{3.12}$$

$$v^m = \frac{K_2 v_2 + K_1 v_1}{K_1 + K_2} + \frac{u_2 - u_1}{K_1 + K_2} \quad . \tag{3.13}$$

When $k_{w_i} = 0$ and $\beta_1 = \beta_2 = \beta$, $K_1 = K_2 = \cot\beta$, the above equations reduce to the simplified form adopted by Wyngaard (1968), viz.

$$u^m = \frac{u_1 + u_2}{2} + \cot\beta \frac{v_2 - v_1}{2} \tag{3.14}$$

$$v^m = \frac{v_1 + v_2}{2} + \tan\beta \frac{u_2 - u_1}{2} \quad . \tag{3.15}$$

The spectral forms of (3.12) and (3.13) can be obtained by using Fourier–Stieltjes expressions about the X-probe centre z_0. For example, u_1 and v_1 can be written as

$$u_1 = \int_{-\infty}^{\infty} e^{i\boldsymbol{k}\cdot\boldsymbol{z}_0} \, e^{i\boldsymbol{k}\cdot\boldsymbol{d}/2} \, A_1 \mathrm{d}Z_1(\boldsymbol{k}) \quad , \tag{3.16}$$

$$v_1 = \int_{-\infty}^{\infty} e^{i\boldsymbol{k}\cdot\boldsymbol{z}_0} \, e^{i\boldsymbol{k}\cdot\boldsymbol{d}/2} \, A_1 \mathrm{d}Z_2(\boldsymbol{k}) \quad , \tag{3.17}$$

where $A_1 = \sin(\boldsymbol{k} \cdot \boldsymbol{\ell}_1/2)/(\boldsymbol{k} \cdot \boldsymbol{\ell}_1/2)$, $\boldsymbol{k}$ is the wavenumber vector and $\boldsymbol{\ell}_1$ is the wire length vector for wire 1. True and measured spectral density tensors are defined by

$$\phi_{ij}(\boldsymbol{k})\mathrm{d}\boldsymbol{k} = \overline{\mathrm{d}Z_i(\boldsymbol{k})\mathrm{d}Z_j^*(\boldsymbol{k})} \tag{3.18}$$

$$\phi_{ij}^m(\boldsymbol{k}, \boldsymbol{\ell})\mathrm{d}\boldsymbol{k} = \overline{\mathrm{d}Z_i^m(\boldsymbol{k}, \boldsymbol{\ell})\mathrm{d}Z_j^{m*}(\boldsymbol{k}, \boldsymbol{\ell})} \quad , \tag{3.19}$$

where $dZ_i(\boldsymbol{k})$ and $dZ_i^m(\boldsymbol{k},\ell)$ are the true and measured Fourier–Stieltjes components, and the asterisk denotes a complex conjugate. For example, $dZ_1^m(\boldsymbol{k},\ell) = e^{j\boldsymbol{k}\cdot\boldsymbol{d}/2}A_1 dZ_1(\boldsymbol{k})$. The spectral forms of (3.12) and (3.13) can now be written as

$$\begin{aligned}(K_1+K_2)^2\phi_{11}^m(\boldsymbol{k}) = {} & [A_2^2K_1^2 + A_1^2K_2^2 + 2K_1K_2A_1A_2\cos(\boldsymbol{k}\cdot\boldsymbol{d})]\phi_{11}(\boldsymbol{k}) \\ & + 2K_1K_2[K_1A_2^2 - K_2A_1^2 + (K_2-K_1)A_1A_2\cos(\boldsymbol{k}\cdot\boldsymbol{d})]\phi_{12}(\boldsymbol{k}) \\ & + K_1^2K_2^2[A_1^2 + A_2^2 - 2A_1A_2\cos(\boldsymbol{k}\cdot\boldsymbol{d})]\phi_{22}(\boldsymbol{k}) \quad , \end{aligned} \tag{3.20}$$

$$\begin{aligned}(K_1+K_2)^2\phi_{22}^m(\boldsymbol{k}) = {} & [A_2^2K_2^2 + A_1^2K_1^2 + 2K_1K_2A_1A_2\cos(\boldsymbol{k}\cdot\boldsymbol{d})]\phi_{22}(\boldsymbol{k}) \\ & + 2[K_2A_2^2 - K_1A_1^2 - (K_2-K_1)A_1A_2\cos(\boldsymbol{k}\cdot\boldsymbol{d})]\phi_{12}(\boldsymbol{k}) \\ & + [A_1^2 + A_2^2 - 2A_1A_2\cos(\boldsymbol{k}\cdot\boldsymbol{d})]\phi_{11}(\boldsymbol{k}) \quad , \end{aligned} \tag{3.21}$$

$$\begin{aligned}(K_1+K_2)^2\phi_{12}^m(\boldsymbol{k}) = {} & [2K_1K_2(A_1^2+A_2^2) + (K_2-K_1)^2A_1A_2\cos(\boldsymbol{k}\cdot\boldsymbol{d})]\phi_{12}(\boldsymbol{k}) \\ & + [K_1A_2^2 - K_2A_1^2 + (K_2-K_1)A_1A_2\cos(\boldsymbol{k}\cdot\boldsymbol{d})]\phi_{11}(\boldsymbol{k}) \\ & + K_1K_2[K_2A_2^2 - K_1A_1^2 - (K_2-K_1)A_1A_2\cos(\boldsymbol{k}\cdot\boldsymbol{d})]\phi_{22}(\boldsymbol{k}) \\ & + j\{(K_1+K_2)A_1A_2\phi_{11}(\boldsymbol{k}) + K_1K_2(K_1+K_2)A_1A_2\phi_{22}(\boldsymbol{k}) \\ & + (K_2^2-K_1^2)A_1A_2\phi_{12}(\boldsymbol{k})\}\sin(\boldsymbol{k}\cdot\boldsymbol{d}) \quad , \end{aligned} \tag{3.22}$$

where $j = \sqrt{-1}$, $A_i = \sin(\boldsymbol{k}\cdot\ell_i/2)/(\boldsymbol{k}\cdot\ell_i/2)$. The true cross-spectrum $\phi_{ij}(\boldsymbol{k})$ is assumed to be symmetrical with respect to its indices so that $\phi_{21}(\boldsymbol{k}) = \phi_{12}(\boldsymbol{k})$. The measured cross-spectrum† $\phi_{12}^m(\boldsymbol{k})$ contains a real part or cospectrum and an imaginary part or quadrature spectrum. Since both parts are affected by the probe geometry, the phase between u and v, which is equal to $\tan^{-1}$ (quadrature spectrum/cospectrum), may also be affected. The second terms on the right of (3.14) and (3.15) were referred to by Wyngaard (1968) as cross-talk terms. Equations (3.20)–(3.22) clearly show the presence of cross-talk between u and v in the measured spectra. For instance, $\phi_{11}^m(\boldsymbol{k})$, equation (3.20), contains contributions from $\phi_{12}(\boldsymbol{k})$ and $\phi_{22}(\boldsymbol{k})$. The cross-talk arises not only because of the finite separation between the hot wires but also as a result of the wire length since the line averaging paths differ for the two wires.

Up to this point, isotropy has not been assumed. However, (3.20)–(3.22) can be used for determining ϕ_{11}^m, ϕ_{22}^m and ϕ_{12}^m only if the true spectra are known. This is feasible if isotropic turbulence is assumed. In this case, the true spectrum $\phi_{ij}(\boldsymbol{k})$ is given by (e.g. Batchelor 1953)

$$\phi_{ij}(\boldsymbol{k}) = \phi_{ij}(k) = \frac{E(k)}{4\pi k^4}(k^2\delta_{ij} - k_ik_j) \quad , \tag{3.23}$$

where $k \equiv (k_1^2 + k_2^2 + k_3^2)^{1/2}$ is the magnitude of $\boldsymbol{k}$ and $E(k)$ is the three-dimensional energy spectrum.

Correction ratios for the one-dimensional spectra $\phi_u^m(k_1)$ and $\phi_v^m(k_1)$, where $\phi_u^m(k_1) = \int\int_{-\infty}^{\infty}\phi_{11}^m(\boldsymbol{k})dk_2dk_3$ and $\phi_v^m(k_1) = \int\int_{-\infty}^{\infty}\phi_{22}^m(\boldsymbol{k})dk_2dk_3$ and for the Reynolds stresses $\overline{u^2}^m$ and $\overline{v^2}^m$ can be introduced, viz.

† To our knowledge, the expression for $\phi_{12}^m(\boldsymbol{k})$ has not been considered in previous analyses.

$$R_{\phi_u}(k_1) = \frac{\phi_u^m(k_1)}{\phi_u(k_1)} = \int\int_{-\infty}^{\infty} \phi_{11}^m(\boldsymbol{k})\mathrm{d}k_2\mathrm{d}k_3 \Big/ \int\int_{-\infty}^{\infty} \phi_{11}(\boldsymbol{k})\mathrm{d}k_2\mathrm{d}k_3 \quad , \tag{3.24}$$

$$R_{\phi_v}(k_1) = \frac{\phi_v^m(k_1)}{\phi_v(k_1)} = \int\int_{-\infty}^{\infty} \phi_{22}^m(\boldsymbol{k})\mathrm{d}k_2\mathrm{d}k_3 \Big/ \int\int_{-\infty}^{\infty} \phi_{22}(\boldsymbol{k})\mathrm{d}k_2\mathrm{d}k_3 \quad , \tag{3.25}$$

$$r_u = \frac{\overline{u^2}^m}{\overline{u^2}} = \int_{-\infty}^{\infty} \phi_u^m(k_1)\mathrm{d}k_1 \Big/ \int_{-\infty}^{\infty} \phi_u(k_1)\mathrm{d}k_1 \quad , \tag{3.26}$$

$$r_v = \frac{\overline{v^2}^m}{\overline{v^2}} = \int_{-\infty}^{\infty} \phi_v^m(k_1)\mathrm{d}k_1 \Big/ \int_{-\infty}^{\infty} \phi_v(k_1)\mathrm{d}k_1 \quad . \tag{3.27}$$

The correction ratios for one-dimensional cospectra $Co_{uv}(k_1)$, where $Co_{uv}(k_1) = \int\int_{-\infty}^{\infty} \phi_{12}(\boldsymbol{k})\mathrm{d}k_2\mathrm{d}k_3$, and $\overline{uv}^m$ are not given since these two quantities are zero for isotropic turbulence. The integrals in (3.24) to (3.27) can be evaluated numerically if $E(k)$ is known. There are several ways in which $E(k)$ can be estimated, each one leading to virtually the same result. One possibility is to use (e.g. Antonia, Browne & Chambers 1984)

$$E(k) = k^2 \left(\frac{\partial^2 \phi_u}{\partial k_1^2}\right)_{k_1=k} - k \left(\frac{\partial \phi_u}{\partial k_1}\right)_{k_1=k} \quad , \tag{3.28}$$

and a known distribution of $\phi_u(k_1)$.

Equations (3.20)–(3.22) take into account the effect of the tangential velocity component and the possible asymmetry of the X-probe. They should be more generally applicable than Wyngaard's analysis which used only a cosine response equation (according to Lomas 1986 this is adequate only when the wire aspect ratio is greater than 600) and assumed symmetry of the X-probe about the flow direction.

4. Correction for homogeneous turbulence

Although the spectral analysis presented in § 3 does not assume isotropy, its practical implementation requires this assumption. Obviously, this assumption will break down near a wall. Therefore, it is not possible to correct the measured spectra of u and v using the results of § 3. However, correction ratios for the Reynolds stresses can be derived directly from (3.12) and (3.13) which should be valid in the wall region since the effect of the mean velocity gradient (e.g. Vukoslavčević & Wallace 1981; Park & Wallace 1992) is small. $\overline{u^2}^m$ and $\overline{v^2}^m$ can be obtained by squaring and then averaging (3.12) and (3.13) respectively while $\overline{uv}^m$ is obtained by multiplying (3.12) and (3.13) and then averaging. The wire length effect is neglected for simplicity. The correction ratios for the Reynolds stresses are as follows:

$$\begin{aligned} r_u &= \frac{\overline{u^2}^m}{\overline{u^2}} \\ &= \{K_1^2 + K_2^2 + 2K_1K_2\rho_{uu}(d) + 2K_1^2K_2^2\frac{\overline{v^2}}{\overline{u^2}}[1 - \rho_{vv}(d)] \\ &\quad - 2K_1K_2(K_2 - K_1)\frac{\overline{uv}}{\overline{u^2}} + 2K_1K_2\frac{\overline{u'v'}}{\overline{u^2}}[K_2\rho_{uv}(d) \\ &\quad - K_1\rho_{vu}(d)]\}/(K_1 + K_2)^2 \quad , \end{aligned} \tag{4.1}$$

$$r_v = \frac{\overline{v^2}^m}{\overline{v^2}}$$

$$= \{K_1^2 + K_2^2 + 2K_1K_2\rho_{vv}(d) + 2\frac{\overline{u^2}}{\overline{v^2}}[1 - \rho_{uu}(d)]$$

$$+ 2(K_2 - K_1)\frac{\overline{uv}}{\overline{v^2}} - 2\frac{\overline{u'v'}}{\overline{v^2}}[K_2\rho_{uv}(d) - K_1\rho_{vu}(d)]\}/(K_1 + K_2)^2 \quad , \tag{4.2}$$

$$r_{uv} = \frac{\overline{uv}^m}{\overline{uv}}$$

$$= \{4K_1K_2 + (K_1 - K_2)\frac{\overline{u^2}}{\overline{uv}} - (K_1 - K_2)\frac{\overline{u^2}}{\overline{uv}}\rho_{uu}(d)$$

$$+ K_1K_2(K_2 - K_1)\frac{\overline{v^2}}{\overline{uv}} + K_1K_2(K_1 - K_2)\frac{\overline{v^2}}{\overline{uv}}\rho_{vv}(d)$$

$$+ (K_2 - K_1)\frac{\overline{u'v'}}{\overline{uv}}[K_2\rho_{uv}(d) - K_1\rho_{vu}(d)]\}/(K_1 + K_2)^2 \quad , \tag{4.3}$$

where ρ_{uu}, ρ_{vv}, ρ_{uv} and ρ_{vu} are correlation coefficients defined as follows:

$$\rho_{uu}(d) = \frac{\overline{u(y,z)u(y,z+d)}}{\overline{u^2}(y)} \tag{4.4}$$

$$\rho_{vv}(d) = \frac{\overline{v(y,z)v(y,z+d)}}{\overline{v^2}(y)} \tag{4.5}$$

$$\rho_{uv}(d) = \frac{\overline{u(y,z)v(y,z+d)}}{u'(y)v'(y)} \tag{4.6}$$

$$\rho_{vu}(d) = \frac{\overline{v(y,z)u(y,z+d)}}{u'(y)v'(y)} \quad . \tag{4.7}$$

Hereafter, the dependence on y is omitted for convenience of writing.

Because of the assumed homogeneity, $\rho_{uv}(d) = \rho_{vu}(d)$. When the asymmetry is small, $K_2 - K_1 \ll K_1$, $K_2 - K_1 \ll K_2$. As a result of the previous approximations, the last two terms on the right of (4.1) and (4.2) can be neglected. In (4.3), the second and third terms on the right cannot be neglected since $\overline{u^2}$ may be considerably greater than $\overline{v^2}$ and $\overline{uv}$, especially near the wall. Nonetheless, the last three terms should be much smaller than the first three and (4.1)–(4.3) may be simplified to

$$r_u = \frac{\left\{K_1^2 + K_2^2 + 2K_1K_2\rho_{uu}(d) + 2K_1^2K_2^2(\overline{v^2}/\overline{u^2})[1 - \rho_{vv}(d)]\right\}}{(K_1 + K_2)^2} \quad , \tag{4.8}$$

$$r_v = \frac{\left\{K_1^2 + K_2^2 + 2K_1K_2\rho_{vv}(d) + 2(\overline{u^2}/\overline{v^2})[1 - \rho_{uu}(d)]\right\}}{(K_1 + K_2)^2} \quad , \tag{4.9}$$

$$r_{uv} = \frac{\left\{4K_1K_2 + (K_1 - K_2)(\overline{u^2}/\overline{uv}) + (K_2 - K_1)(\overline{u^2}/\overline{uv})\rho_{uu}(d)\right\}}{(K_1 + K_2)^2} \quad . \tag{4.10}$$

Only spanwise homogeneity has been assumed in (4.8)–(4.10). These equations should be applicable everywhere in the flow. One exception is the use of (4.10) on the channel centreline, where $\overline{uv}$ is zero (by symmetry); in this case, the expression for $\overline{uv}^m$ should still be valid. The evaluation of these ratios requires a knowledge of the two-point correlation coefficients $\rho_{uu}(d)$ and $\rho_{vv}(d)$ and parameters $\overline{u^2}/\overline{v^2}$ and $\overline{u^2}/\overline{uv}$. The available DNS database (e.g. Kim *et al.* 1987) and data provided by Dr J. Kim (private communication, 1993) can be used for obtaining this information. An encouraging feature of the data is the almost negligible dependence of $\rho_{uu}(d^+)$ and $\rho_{vv}(d^+)$ on the Reynolds number in the wall region. This suggests that the proposed correction procedure should be reasonably accurate when it is applied to experimental data obtained at higher Reynolds numbers than those at which the simulations were made. Without DNS data, $\rho_{uu}(d)$ can be measured with two parallel hot wires, though with some difficulty when d is very small. The accurate measurements of $\rho_{vv}(d)$ would pose some difficulty especially in the wall region. However, it may be possible to use the self-similarity idea of Hunt *et al.* (1987) to determine the shape of the correlation ρ_{vv} in this region. These authors found that v-correlations between two points y, y_1 ($y_1 > y$) assume an approximately self-similar form $\overline{v(y)v(y_1)}/\overline{v^2(y_1)} = f(y/y_1)$, independently of y_1; the ratio $\overline{v(y,d)v(y,0)}/\overline{v(y,0)v(y_1,0)}$ is also self-similar and independent of z. A knowledge of these ratios should allow estimates of $\rho_{vv}(d)$ to be made in the wall region.

5. Results for isotropic turbulence

The correction ratios R_{ϕ_u}, R_{ϕ_v}, r_u and r_v are calculated for isotropic turbulent flows via (3.24)–(3.27) respectively. $E(k)$ was calculated from the DNS data for ϕ_u via (3.28). Practically the same distribution for $E(k)$ resulted when a distribution of ϕ_u, measured with a single hot wire, was used as the input to the calculation.

Figure 2(*a,b*) shows the effect of wire length on the spectral correction ratios R_{ϕ_u} and R_{ϕ_v} for different values of k_1^* ($k_1^* = k_1\eta$; η is the Kolmogorov length scale $\nu^{3/4}/\bar{\epsilon}^{1/4}$; $\bar{\epsilon}$ is the average energy dissipation rate; η is about 0.38 mm at the channel centreline and 0.20 mm near the wall; the asterisk denotes normalization by η and the Kolmogorov velocity scale $U_K \equiv \nu^{1/4}\bar{\epsilon}^{1/4}$) when $\beta_1 = \beta_2 = 45°$. In this case, k_{w_1} and k_{w_2} are set equal to 0.2 when evaluating R_{ϕ_u} and R_{ϕ_v} from (3.24) and (3.25). It should be noted that the tangential cooling coefficient k_w in the cooling equations normally depends on the effective angle, α, between the velocity vector and wire axis, the type of probe and the mean velocity. Allowing for the experimental scatter, available data for k_w (e.g. Champagne, Sleicher & Wehrman 1967; Jörgensen 1971; Bruun 1972; Andreopoulos 1983; Bruun & Tropea 1985; Hishida & Nagano 1988) show that k_w decreases almost linearly with α and varies significantly for different probe types, although the velocity dependence is relatively small. For the present probe type, which is similar to that (55F11) of Jörgensen (1971) or that (55P01) of Bruun & Tropea (1985), k_w decreases between about 0.3 when $\alpha = 20°$ and 0.1 when $\alpha = 80°$. It is therefore inappropriate to choose a constant value of k_w for different effective angles (this will be discussed later). Strictly, k_w varies instantaneously with α in turbulent flows; it would be difficult to include the instantaneous variation of k_w into the calibration procedure and the spectral expressions. For simplicity, we have assumed an average value of k_w for an average effective angle (e.g. Bruun & Tropea 1985; Browne *et al.* 1988). In all the calculations, average values of 0.2 and 0.24 were used for k_w, corresponding to average values of α of 45° (or $\beta = 45°$) and 30° (or $\beta = 60°$) respectively.

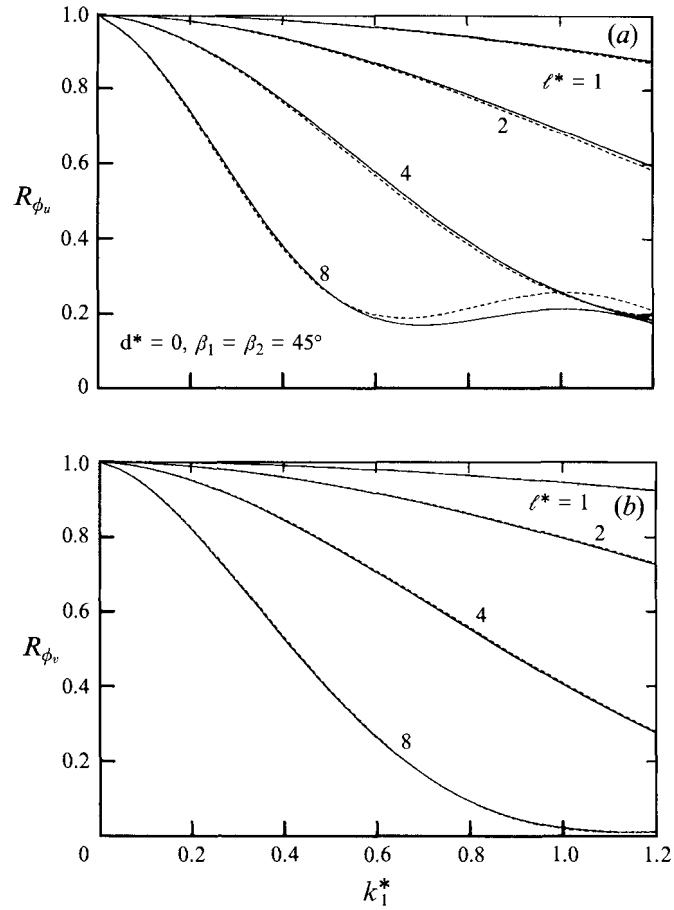

FIGURE 2. Effect of wire length on the spectral correction ratios R_{ϕ_u} and R_{ϕ_v}. (*a*) R_{ϕ_u}; (*b*) R_{ϕ_v}. —, Calculation using (3.20) and (3.21); - - -, calculation using the spectral expressions of Wyngaard (1968).

Figure 2(*a*,*b*) also shows the calculations of R_{ϕ_u} and R_{ϕ_v} using Wyngaard's spectral expressions (i.e. equation (15) in Wyngaard 1968). The separation is set equal to zero to focus only on the length effect. The wire length attenuates ϕ_u and ϕ_v at all wavenumbers, the attenuation being generally larger at higher wavenumbers. There is very little difference between the distributions of R_{ϕ_u}, R_{ϕ_v} calculated from the present spectral expressions and those obtained from Wyngaard's spectral expressions (with the same $E(k)$). When the separation is taken into account, ϕ_u (figure 3*a*) is overestimated for $k_1^* \gtrsim 0.15$ and underestimated for $k_1^* \lesssim 0.15$, these changes increasing with separation. Opposite trends are observed for ϕ_v (figure 3*b*). Figure 3 also shows the distributions of R_{ϕ_u} and R_{ϕ_v}, calculated from Wyngaard's spectral expressions. In the latter case, R_{ϕ_u} is overestimated and R_{ϕ_v} is underestimated at all wavenumbers, indicating that the yaw factor has a non-negligible effect on R_{ϕ_u} and R_{ϕ_v}. As a check of the integrations involved in (3.24) and (3.25), calculations were also carried out with $\beta_1 = \beta_2 = 45°$ and $k_{w_1} = k_{w_2} = 0$ in (3.20) and (3.21). As noted earlier, these equations become identical to those of Wyngaard. The calculations (not shown here) for $\ell = d$ and $\ell = 2d$ are also in quite good agreement with those of Wyngaard.

The large difference between the behaviour of $R_{\phi_u}(k_1)$ and $R_{\phi_v}(k_1)$ is due to the

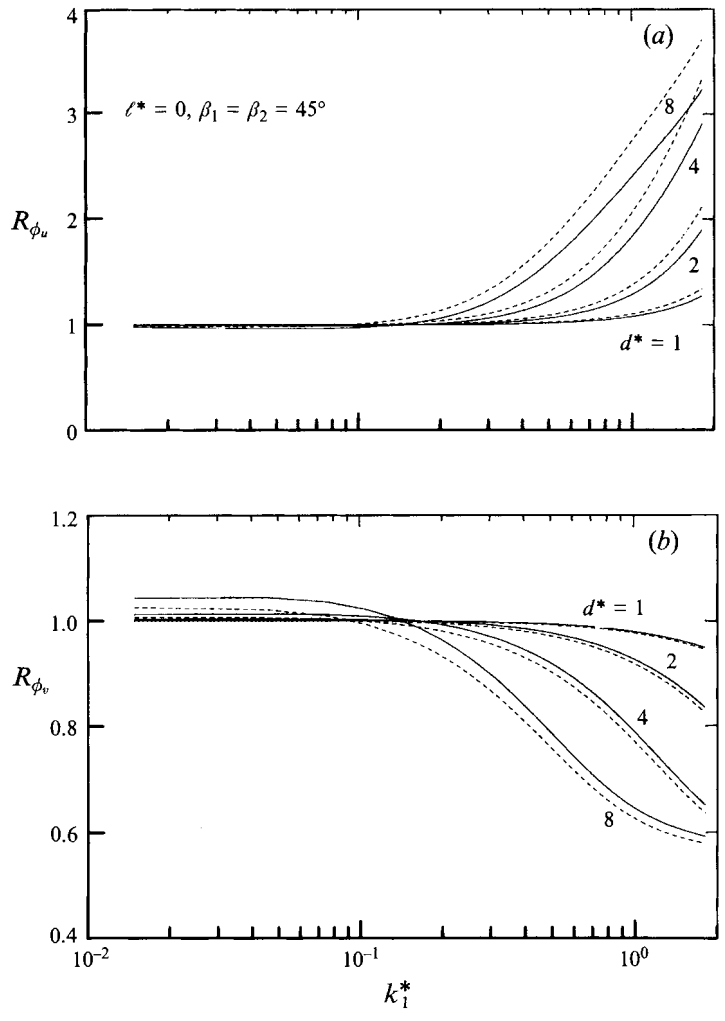

FIGURE 3. Effect of wire separation on the spectral correction ratios R_{ϕ_u} and R_{ϕ_v}. (*a*) R_{ϕ_u}; (*b*) R_{ϕ_v}. —, Calculation using (3.20) and (3.21); - - -, calculation using the spectral expressions of Wyngaard (1968).

line averaging, i.e. $A_1 = A_2 = 1$, the expressions for $\phi_u^m(k_1)$ and $\phi_v^m(k_1)$ simplify to (for $\beta_1 = \beta_2 = 45°$ and $k_{w_1} = k_{w_2} = 0$)

$$\phi_u^m(k_1) = \tfrac{1}{2}\phi_u(k_1) + \tfrac{1}{2}\phi_v(k_1) + \tfrac{1}{2}\int\int_{-\infty}^{\infty} \cos(\boldsymbol{k}\cdot\boldsymbol{d})[\phi_{11}(k) - \phi_{22}(k)]\mathrm{d}k_2\mathrm{d}k_3 \quad , \tag{5.1}$$

$$\phi_v^m(k_1) = \tfrac{1}{2}\phi_u(k_1) + \tfrac{1}{2}\phi_v(k_1) - \tfrac{1}{2}\int\int_{-\infty}^{\infty} \cos(\boldsymbol{k}\cdot\boldsymbol{d})[\phi_{11}(k) - \phi_{22}(k)]\mathrm{d}k_2\mathrm{d}k_3 \quad . \tag{5.2}$$

These expressions differ from those given by Wyngaard, which did not contain the integral terms (as will be shown below, their values are not negligible). When estimating these integrals, it is always possible to find a constant ζ $(0 \leqslant \zeta \leqslant 1)$ so that

$$\int\int_{-\infty}^{\infty} \cos(\boldsymbol{k}\cdot\boldsymbol{d})[\phi_{11}(k) - \phi_{22}(k)]\mathrm{d}k_2\mathrm{d}k_3 = \zeta[\phi_u(k_1) - \phi_v(k_1)] \quad . \tag{5.3}$$

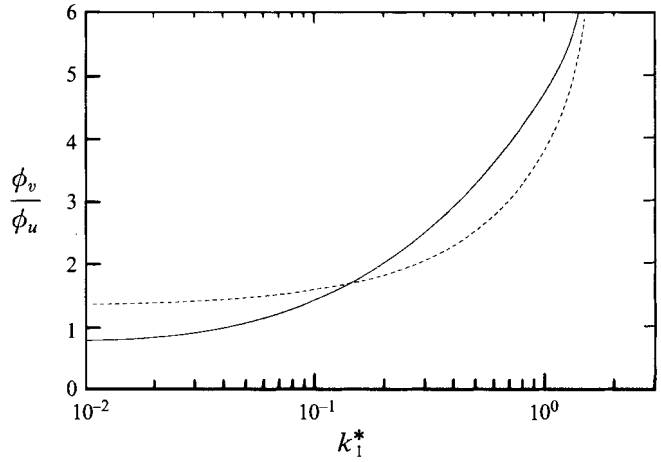

FIGURE 4. Ratio of spectra of v and u: —, present; - - -, Wyngaard (1968).

The resulting correction ratios are

$$R_{\phi_u} = \tfrac{1}{2}(1+\zeta) + \tfrac{1}{2}(1-\zeta)\,\phi_v/\phi_u \tag{5.4}$$

$$R_{\phi_v} = \tfrac{1}{2}(1+\zeta) + \tfrac{1}{2}(1-\zeta)\,\phi_u/\phi_v \quad . \tag{5.5}$$

when $d = 0$, $\zeta = 1$ and $R_{\phi_u} = R_{\phi_v} \equiv 1$. The ratio ϕ_v/ϕ_u, evaluated from the DNS distribution for $E(k)$, is compared in figure 4 with Wyngaard's (1968) calculation obtained with Pao's (1965) form of $E(k)$.

At $k_1^* = 0$, this ratio assumes a value of $\frac{1}{2}$, viz.

$$\frac{\phi_v}{\phi_u} = \frac{\frac{1}{2}\displaystyle\int_{k_1}^{\infty}\left(1-\frac{k_1^2}{k^2}\right)\frac{E(k)}{k}\mathrm{d}k}{\frac{1}{4}\displaystyle\int_{k_1}^{\infty}\left(1+\frac{k_1^2}{k^2}\right)\frac{E(k)}{k}\mathrm{d}k} = \frac{\frac{1}{2}\displaystyle\int_{0}^{\infty}\frac{E(k)}{k}\mathrm{d}k}{\displaystyle\int_{0}^{\infty}\frac{E(k)}{k}\mathrm{d}k} = \frac{1}{2} \quad , \tag{5.6}$$

which is a consequence of isotropy. The ratio increases rapidly with increasing k_1^*. The discrepancy between the two calculations at high wavenumber is due to the difference between the two distributions of $E(k)$ (e.g. Antonia *et al.* 1993). The familiar value of 4/3 for the inertial range, as predicted by Wyngaard (1968), is not observed in the present calculation since the present $\phi_u(k_1)$ data do not exhibit an inertial range (due to the low Reynolds number). In the extreme case when $\zeta = 0$, $R_{\phi_u} = 3/4$ and $R_{\phi_v} = 3/2$ for $k_1^* = 0$ while $R_{\phi_u} \to \infty$ and $R_{\phi_v} \to 1/2$ as $k_1^* \to \infty$. This means that for a symmetrical 45° X-probe, ϕ_u would be underestimated (maximum 25%) at small k_1^* and greatly overestimated at large k_1^*; ϕ_v would be overestimated (as much as 50%) at small k_1^* and underestimated (maximum 50%) at large k_1^*. This behaviour is clearly reflected in the distributions of figure 3. It should be noted that the R_{ϕ_u} and R_{ϕ_v} distributions (figures 2 and 3) are for $\beta_1 = \beta_2 = 45°$ only. When β_1 and β_2 increase, the general shapes of R_{ϕ_u} and R_{ϕ_v} are similar to those for $\beta_1 = \beta_2 = 45°$, but the errors in ϕ_u and ϕ_v are larger (these results are not shown here).

Figure 5 shows the correction ratios of $\overline{u^2}$ and $\overline{v^2}$ for $\beta_1 = \beta_2 = 45°$ and 60° and those evaluated using Wyngaard's spectral expressions. The wire length has been neglected since ℓ^* is normally in the range 1 to 4, and the effect on $\overline{u^2}$, $\overline{v^2}$ is small ($\leqslant 1.5\%$). The ratios depend on the magnitudes of the effective angles.

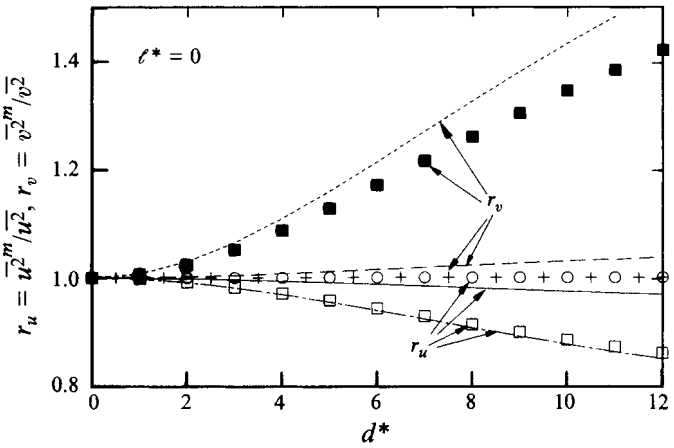

FIGURE 5. Distributions of the calculated correction ratios r_u and r_v (lines) and comparison with the analysis of Wyngaard (1968)(symbols). r_u: —, - - -, □, ○. r_v: - - -, – –, +, ■ $\beta_1 = \beta_2 = 45°$: —, – –, +, ○. $\beta_1 = \beta_2 = 60°$: - - -, - - -, ■, □.

The combination $\beta_1 = \beta_2 = 45°$ appears to be optimum since r_u and r_v are nearly equal to 1, i.e. the measurements should be virtually error-free. Different angle combinations may however result in significant errors. For the same separation, the combination $\beta_1 = 60°$ $\beta_2 = 60°$ may result in larger experimental errors than the use of $\beta_1 = \beta_2 = 45°$. For example, figure 5 shows that, for $d^* = 4$ and $d^* = 8$, the values of r_u for the first combination are about 2% and 8% smaller than for the second. For the first combination, the values of r_v are about 10% and 30% bigger than for the second. For a particular effective angle, the choice of k_w may affect the calculated correction ratios. The present calculations show that an increase in k_w value generally results in an increase in r_v but a decrease in r_u. The difference is more pronounced for r_v. Thus, the use of a constant value of k_w for different effective angles may result in errors in the correction ratios due to the effective angle dependence of k_w (e.g. for $d^* = 8$ and $\beta_1 = \beta_2 = 60°$, r_v may be underestimated by 8% if $k_w = 0.2$ is used instead of 0.24). In general, Wyngaard's spectral expressions underestimate r_v but overestimate r_u. This indicates that the inclusion of k_w in (3.1) has a non-negligible effect on r_u and r_v. Especially for a conventional X-probe, Wyngaard's results suggest that $\overline{u^2}$ and $\overline{v^2}$ are measured correctly (since $r_u = r_v \equiv 1$ for all separations when $\beta_1 = \beta_2 = 45°$). However, Browne *et al.* (1988) reported that Wyngaard's calculation resulted in an increase in $\overline{u^2}^m$ as d increased (a trend opposite to their measurements). To check this conclusion, calculations were done using Wyngaard's spectral expressions and including wire length effects ($\ell = d$ and $\ell = 2d$). It was found that r_u and r_v are less than 1, the deficit tending to increase with increasing ℓ, indicating that both $\overline{u^2}$ and $\overline{v^2}$ are underestimated. This invalidates Browne et al.'s observation. The authors were apparently misled by the significant increase at high wavenumbers (figure 3); although the attenuation of ϕ_u^m at small wavenumbers is relatively small, its contribution to $\overline{u^2}^m$ is dominant. Browne *et al.*'s conclusion that Wyngaard's corrections are not suitable for correcting X-probe data for the effect of wire separation is also incorrect since it will be shown below that a suitably modified version of Wyngaard's analysis is in fact closely validated by experiment.

In order to check (3.20), (3.21) (3.22), measurements were made at the channel centreline where isotropy is nearly satisfied, with respect to both the large scales

and, more especially, the small scales (Antonia & Kim 1992, 1993). In the present experiment, we concentrated on measuring the Reynolds stresses in the (x, y)-plane, i.e. the plane of mean shear, although the analysis in § 3 applies equally well to the (x, z)-plane. Measurements were first made to check the effect of varying d on the effective wire angles. These angles were nearly constant ($\pm 5\%$) when the separation d^* is in the range 1 to 10. However, at very small separations ($d^* \lesssim 1$), the effective angles decrease by 30%, probably due to thermal wake interference between the wires. To avoid this extraneous influence, only separations in the range of $d^* \geqslant 1$ can be used.

Experiments were made for the following combinations : $\beta_1 = 45°$, $\beta_2 = 45°$ (Case A); $\beta_1 = 48°$, $\beta_2 = 55°$ (Case B); $\beta_1 = 54°$, $\beta_2 = 60°$ (Case C).

Figures 6*a* and 6*b* show measured and calculated values of r_u and r_v for the three cases. In the calculations, k_{w_1} and k_{w_2} are set equal to 0.2 for Case A; $k_{w_1} = 0.21$, $k_{w_2} = 0.23$ for Case B and $k_{w_1} = 0.23$, $k_{w_2} = 0.24$ for Case C. The wire length effect has been neglected in the calculations (for the present experiments, the length is about 1.5η and the errors in $\overline{u^2}$ and $\overline{v^2}$ would be less than 0.5%). The denominator, in (3.26) was measured with a single hot wire. Since the wire length is small ($1.5\eta - 3.0\eta$), the measured value can be identified with the true value. The denominator in (3.27) is difficult to obtain. However, since the X-probe values of $\overline{u^2}^m$ in the range $d^* = 2 \sim 3$ were very close to those from a single hot wire, and the ratio $\overline{v^2}/\overline{u^2}$ in this range agrees well with the corresponding DNS data, we have assumed that $\overline{v^2}^m \simeq \overline{v^2}$ for this range. The calculations agree with the measurements in the range $d^* = 2 \sim 8$, in support of the modified form of Wyngaard's analysis. Figure 6(*a*,*b*) also shows that, for a given value of d^*, the larger the effective angle, the larger the errors in the stresses. This suggests that a symmetrical 45° probe should be preferred to the other configurations (with the rider that the cone angle of the instantaneous velocity vector does not exceed 45°, e.g. Antonia *et al.* 1992). The rapid increase in the measurements for $d^* \lesssim 2$ is probably due to the interference between the wires and their supports and the possible contamination from electronic noise. This increase is spurious and underlines the need to avoid separations smaller than $d^* \lesssim 2$ if the Reynolds stresses are to be estimated reliably. Figure 6*c* shows the measured values of $\overline{u^+v^+}^m$ (in general, the superscript + denotes normalization by wall variables : the friction velocity U_τ, and the kinematic viscosity ν) as a function of d^*. The rapid increase is again observed at small separations, but the effect of d^* is very small when $d^* \geqslant 2$; for the three cases, $\overline{u^+v^+}^m$ is nearly constant and close to zero (the expected value on the channel centreline).

Figure 7 shows measured ($d^* = 4$) and corrected one-dimensional spectra of u and v for Case A. The corrected spectra were obtained by dividing the measured spectral densities by the ratios R_{ϕ_u} and R_{ϕ_v}, calculated from (3.24) and (3.25). For high wavenumbers, $\phi_u^m(k_1)$ is overestimated while $\phi_v^m(k_1)$ is underestimated. It was also verified, from the variable separation experiment, that the errors increase with separation. The corrected spectral distributions (not shown) collapse very nearly onto one curve, which corroborates the present modification.

6. Results in the wall region

In the wall region, (4.8), (4.9) and (4.10) can, in principle, be used to correct the measured data. The DNS two-point correlation coefficients ρ_{uu} and ρ_{vv} are shown in figure 8 at $y^+ = 15$ and 40 (the two locations at which measurements were made) as a function of the spanwise separation d. Included in figure 8 are the osculating

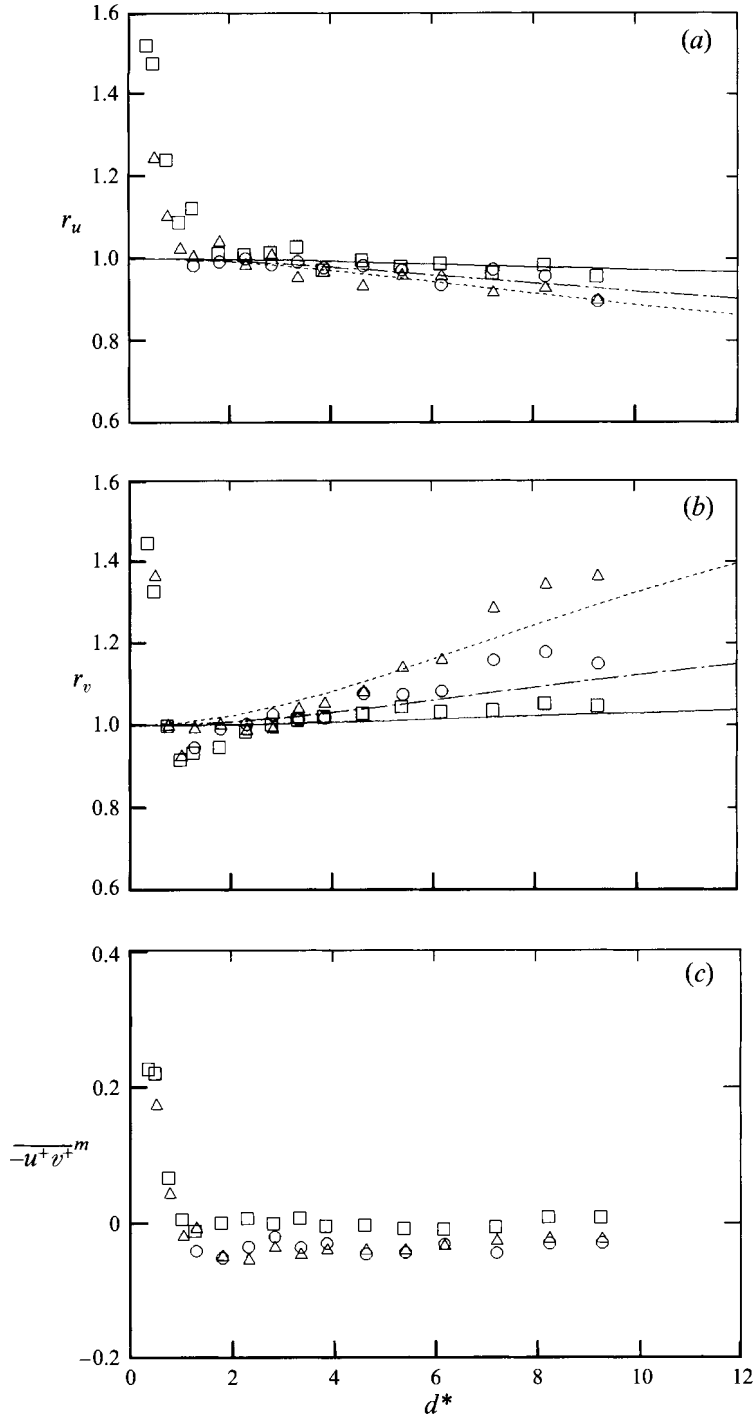

FIGURE 6. Dependence of r_u, r_v and $-\overline{u^+v^+}^m$ on the separation. Measurement: symbols; calculation: lines. Case A: —, □. Case B: – – –, ○. Case C: - - -, △.

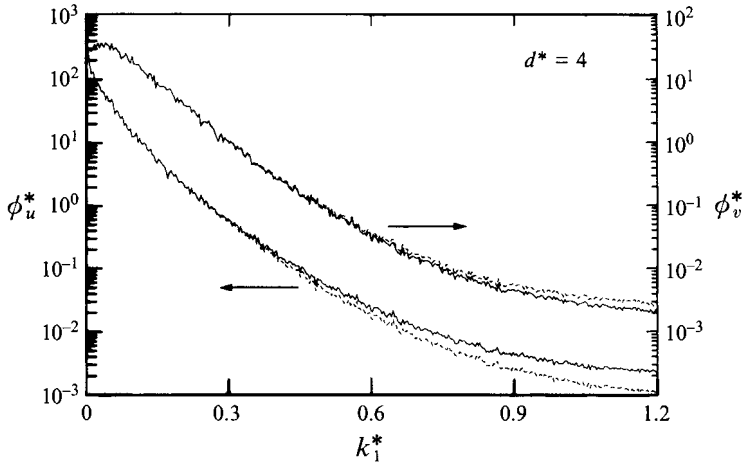

FIGURE 7. Corrected and uncorrected spectra of u and v for Case A. Corrected: - - -; uncorrected: —.

parabolae described by the approximate (homogeneous turbulence) relations (e.g. Batchelor 1953)

$$\left.\begin{aligned} \rho_{uu}(d) &= 1 - d^2/2\lambda_u^2 \\ \rho_{vv}(d) &= 1 - d^2/2\lambda_v^2 \end{aligned}\right\}, \tag{6.1}$$

where $\lambda_u \equiv [\overline{u^2}/\overline{(\partial u/\partial z)^2}]^{1/2}$ and $\lambda_v \equiv [\overline{v^2}/\overline{(\partial v/\partial z)^2}]^{1/2}$ are the Taylor microscales of u and v in the z-direction. Also shown in figure 8 are the calculations of ρ_{uu} or ρ_{vv} obtained from the isotropic relation (e.g. Batchelor 1953)

$$\rho_{uu}(d) = \rho_{vv}(d) = \rho_{ww}(d) + \frac{d}{2}\frac{\partial \rho_{ww}(d)}{\partial d}, \tag{6.2}$$

where $\rho_{ww}(d)$ is the 'longitudinal' correlation coefficient, i.e. the correlation coefficient between spanwise velocity fluctuations in the spanwise direction. The DNS data for ρ_{ww} are used in (6.2). One does not expect isotropy to be satisfied in the wall region and, in this context, the inequality between ρ_{uu} and ρ_{vv} (in figure 8) is not surprising. It is somewhat surprising however that (6.2) satisfies the data for ρ_{uu} remarkably well at both y^+ values. This agreement appears to be associated with the homogeneity of the velocity field in the (x, z)-plane. (Note that ρ_{uu} exhibits a local minimum near $d^+ = 60$, which is reasonably consistent with the expected spanwise wavelength of about 100 wall units for low-speed streaks). The osculating parabolae in figure 8 clearly indicate that the magnitudes of λ_u, λ_v and λ_w are different ($\lambda_v < \lambda_w < \lambda_u$). Such a difference raises doubt on the approach of Westphal (1990) who used (6.1) and assumed a universal value for the Taylor microscale. While (6.1) is correct in the limit of $d \to 0$, it is not an adequate approximation to ρ_{uu} or ρ_{vv} for typical values of d (e.g. $d^* = 5$ corresponds to $d^+ = 9$ at $y^+ = 15$; this would result in ρ_{vv} being overestimated by about 30% if the value of λ_u is used).

In order to check the validity of (4.8)–(4.10), an experiment was also made in the wall region. Figure 9 shows the comparison between the measured and calculated distributions of r_u, r_v and r_{uv} at $y^+ = 15$ and 40 respectively (for the measurements, $\beta_1 = 45°$ and $\beta_2 = 49°$). The DNS data for ρ_{uu} and ρ_{vv} were used in the calculation and the wire length effect was neglected. (The centreline distributions of r_u and r_v are also shown in figure 9, these quantities being calculated from the DNS data of

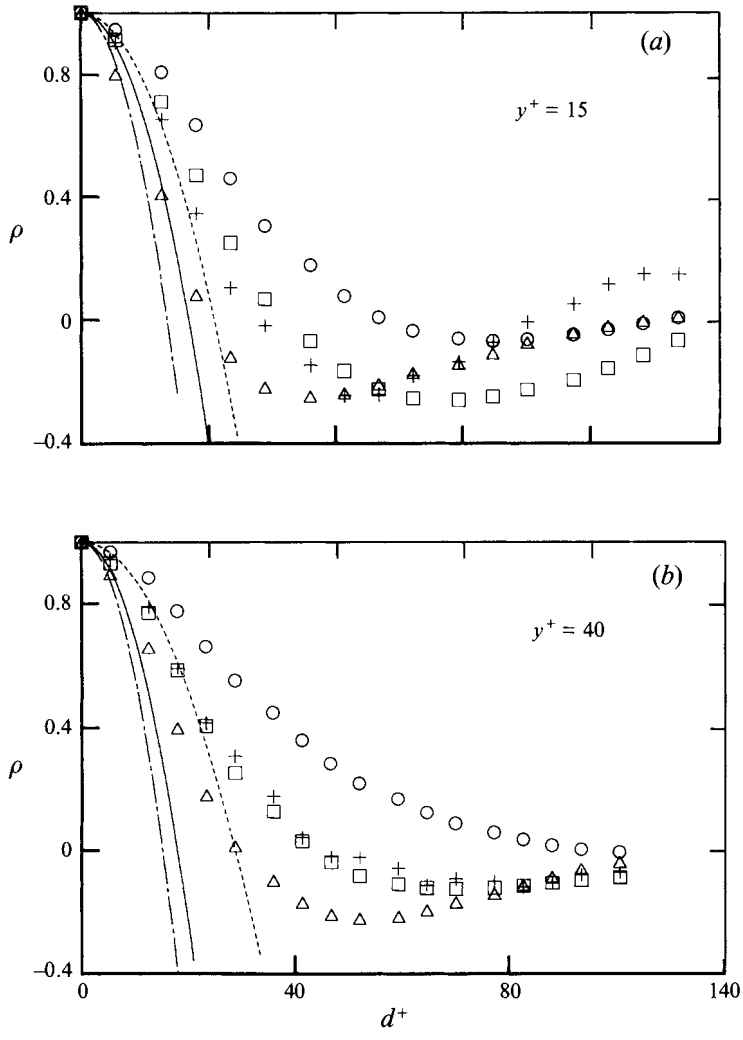

FIGURE 8. Dependence of DNS correlation coefficients on spanwise separation. (*a*) $y^+ = 15$; (*b*) $y^+ = 40$. —, (6.1), $\lambda = \lambda_u$ - - -, (6.1), $\lambda = \lambda_w$ – – –, (6.1), $\lambda = \lambda_v$ ○, ρ_{ww}; □, ρ_{uu}; △, ρ_{vv}; +, calculated ρ_{uu} via (6.2).

ρ_{uu} and ρ_{vv} at $y^+ = 180$. The centreline r_u and r_v distributions are in reasonable agreement with isotropic calculations, based on (6.2) and the DNS data for ρ_{ww}).

The agreement between the measured and calculated distributions of r_u and r_v at $y^+ = 180$ (not shown here) is quite good, suggesting that (4.8) and (4.9) are valid in the central region of the flow. But the centreline distributions of r_u and r_v cannot be used in the wall region, especially for $\overline{v^2}^m$, since the distributions greatly underestimate r_v but overestimate r_u. However, at $y^+ = 15$ and 40, there is good agreement between the calculated and measured distributions of r_u and r_v, providing support for the approach outlined in §4.

The longitudinal Reynolds stress $\overline{u^2}$ (figure 9*a*) is underestimated when $d^* \gtrsim 2$. From (4.8), r_u can be approximated by $1 - 2K_1K_2/(K_1 + K_2)^2[1 - \rho_{uu}(d)]$, since the last term of (4.8) is usually much smaller than the other terms ($\overline{v^2}/\overline{u^2} \ll 1$) and can

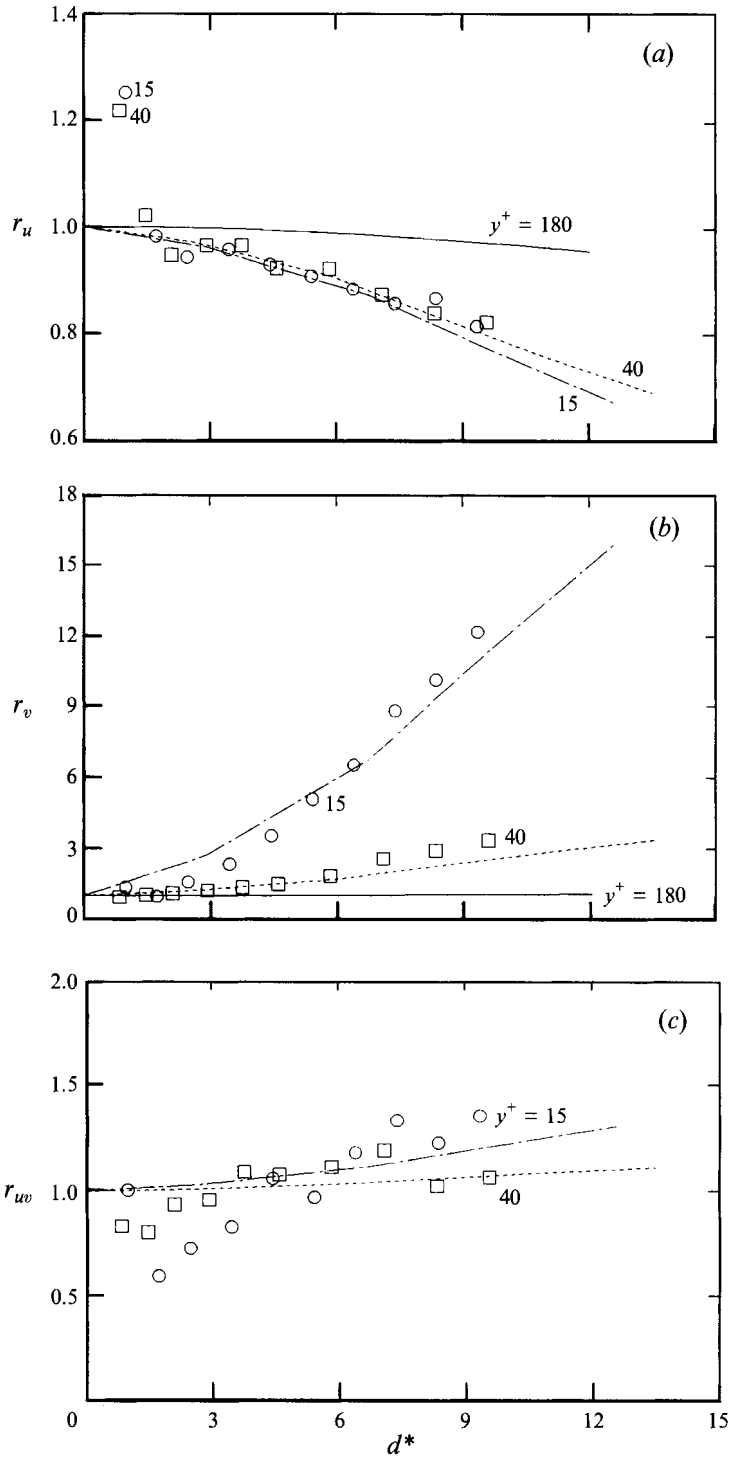

FIGURE 9. Comparison between measurement and calculation of the correction ratios r_u, r_v and r_{uv}. (*a*) r_u; (*b*) r_v; (*c*) r_{uv}. Measurement: symbols; calculation: lines. $y^+ = 180$: —— $y^+ = 40$: - - -, □ $y^+ = 15$: – – –, ○.

be ignored, especially near the wall. It follows that r_u is always less than 1, i.e. $\overline{u^2}$ is always underestimated. The variation of r_u with d is also justified by the experimental data. For a given separation, the amount by which $\overline{u^2}$ is underestimated increases slightly as the wall is approached, since $\rho_{uu}(d)$ changes only slightly for different values of y^+ (figure 8). In the case of $\overline{v^2}$, the cross-talk term is very large, because $\overline{u^2}/\overline{v^2} \gg 1$. Consequently, r_v is always greater than 1 and $\overline{v^2}$ is always overestimated (by 180% at $y^+ = 40$ and 600% at $y^+ = 15$ when $d^* = 6$). This amount increases as d increases. As $y^+ \to 0$, r_v increases since $\overline{u^2}/\overline{v^2}$ increases (figure 9*b*). Although the measured values of r_{uv} (figure 9c) are more scattered than those for r_u and r_v, the generally upward trend with increasing separation seems consistent with the calculation. As $y^+ \to 0$, both measured and calculated values increase due to the slight asymmetries of the probe.

To compare the present procedure with the corrections proposed by Westphal (1990) and Suzuki & Kasagi (1990), the present calculations of r_u, r_v and r_{uv}, together with the corresponding results calculated from Westphal's expressions, and those obtained from Suzuki & Kasagi's expressions (r_{uv} was not given in the latter case; the DNS data of ρ_{uu} was used) are shown in figure 10 for $y^+ = 15$. The r_u distribution (figure 10*a*) is underestimated both by the correction of Suzuki & Kasagi and, more especially by that of Westphal. For r_v (figure 10*b*), Westphal's approach overestimates the distribution (40% at $d^* = 6$) while Suzuki & Kasagi's approach underestimates it (40% at $d^* = 6$). For r_{uv} (figure 10*c*), Westphal's expression yields a trend (a decrease in r_{uv} as d^* increases) which is opposite to that of the present calculation and measurements.

The above observations suggest that both Westphal and Suzuki & Kasagi's procedures do not correct the measured Reynolds stresses reasonably. The reasons for the relatively poor performance of Westphal's approach are probably the inadequacy of the assumption $\lambda_u = \lambda_v = \lambda_{uv}$ and the incorrect expression for $\overline{uv}^m$ (Westphal 1990). In Suzuki & Kasagi's approach, the neglect of the ρ_{vv} term may lead to significant errors in the correction ratios. Further, these two approaches, which do not account for possible asymmetries of the X-probe, become unreliable when the X-probe is not symmetrical.

7. Results with a fixed separation

While the variable separation experiments are important for obtaining reliable Reynolds stress data, this approach is time consuming and its implementation would be impractical if Reynolds stress profiles are to be obtained on a routine basis. Indeed, the common approach is to traverse a fixed separation X-probe across the flow. The present data (figures 6 and 9) suggest that a reasonable choice for d^* would be 2 to 3. In particular, Browne *et al.*'s (1988) recommendation that d^* should be less than 3 is incorrect since data obtained with $d^* < 1$ are unreliable (figure 6).

In the present experiment, a value of $d = 0.65$ mm was used for the fixed separation X-probe, corresponding to a variation in d^* between 3.2 at $y^+ = 5$ and 1.8 at $y^+ = 180$ (channel centreline). The measured distributions of $\overline{u^2}$, $\overline{v^2}$ and $\overline{uv}$ are plotted in figure 11 as a function of y^+. Also shown are the corresponding DNS data ($h^+ = 180$, Kim *et al.* 1987), LDV data ($h^+ = 169$, Wei & Willmarth 1989) and PIV data ($h^+ = 205$, Nishino & Kasagi 1989). The values of $\overline{v^2}$ reported by Antonia *et al.* (1991; see also Antonia *et al.* 1992), with an X-probe ($d = 0.35$ mm; $d^* = 0.9$ at $y^+ = 180$ and $d^* = 1.5$ at $y^+ = 5$) in the same flow as for the present experiment, are included in figure 11*b*.

Figures 11(*a*) ($\overline{u^2}$) and 11(*c*) ($\overline{uv}$) show that the level of agreement between the present measurements and the other data (LDV, PIV, DNS) is quite reasonable,

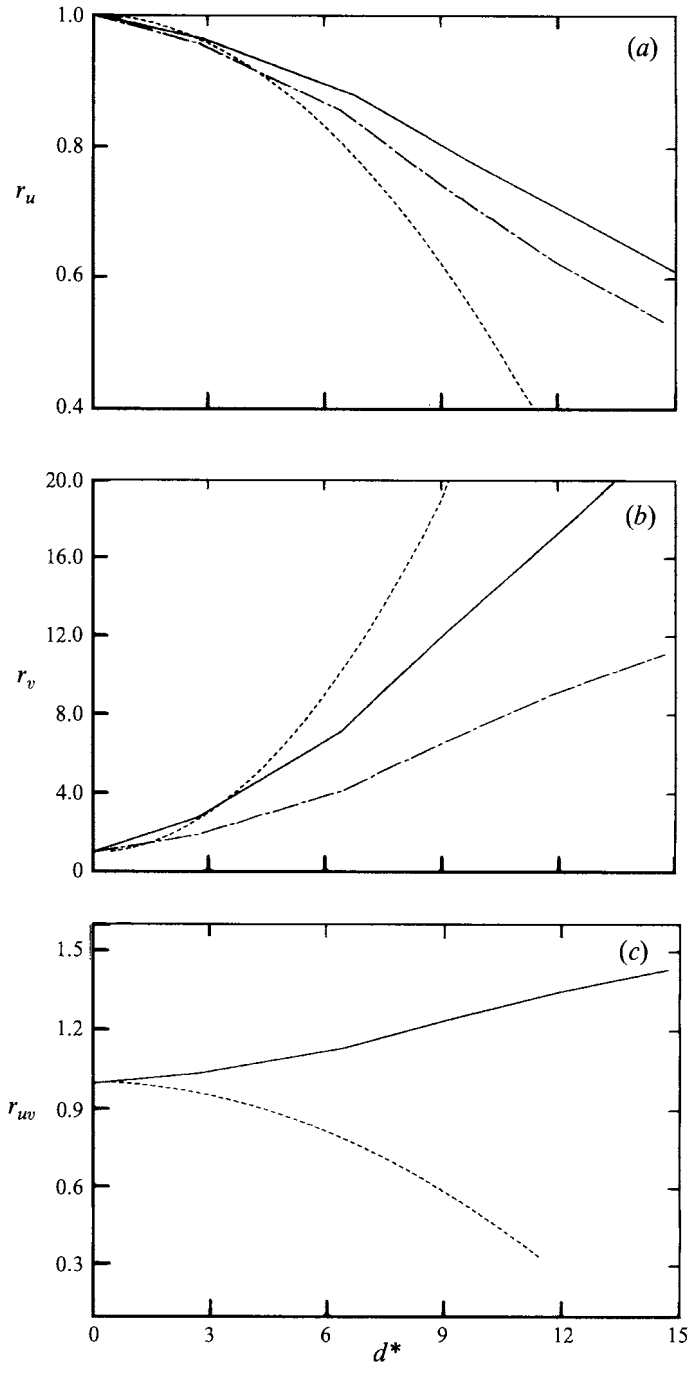

FIGURE 10. Calculated distributions of the correction ratios r_u, r_v and r_{uv} at $y^+ = 15$. (*a*) r_u; (*b*) r_v; (*c*) r_{uv}: —, present; - - -, Westphal (1990); – – –, Suzuki & Kasagi (1990).

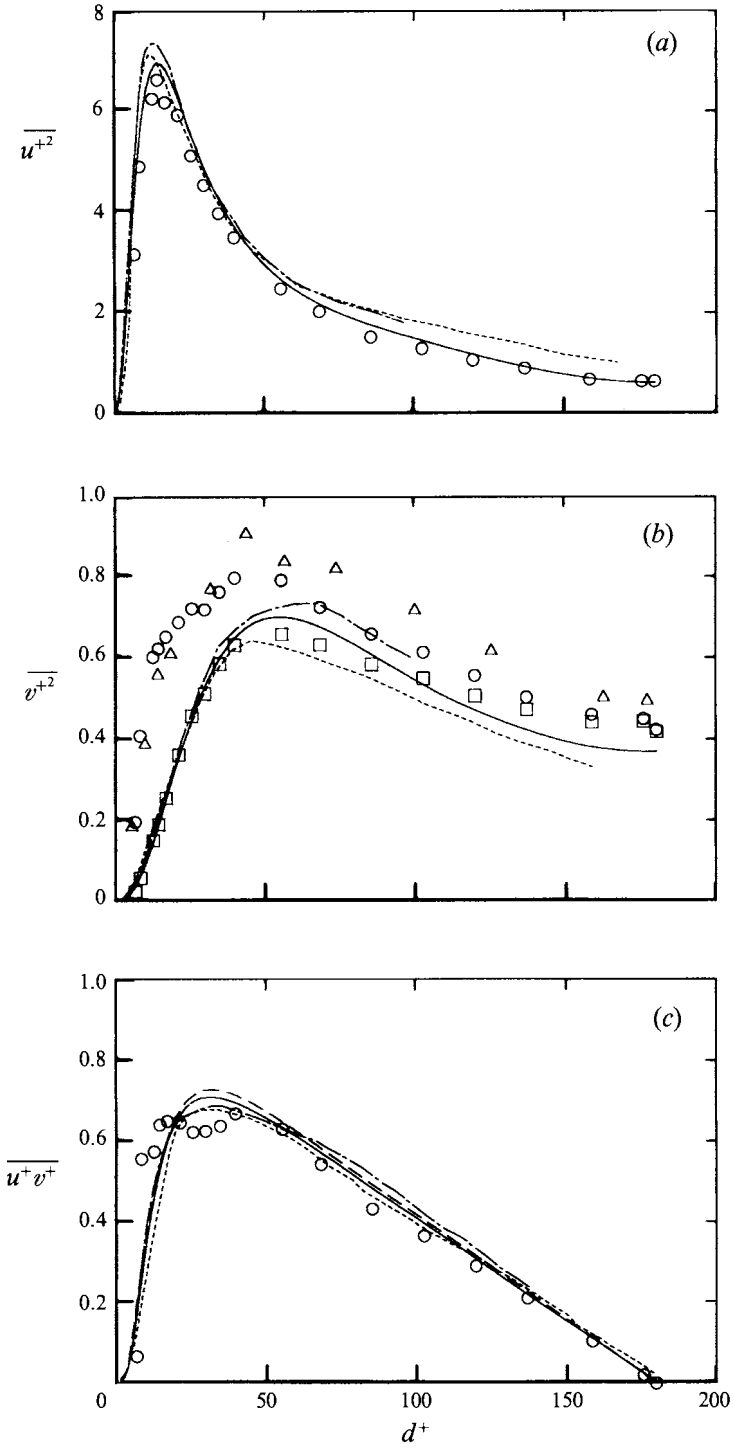

FIGURE 11. Distributions of $\overline{u^{+2}}$, $\overline{v^{+2}}$ and $-\overline{u^+v^+}$; comparison between different types of measurement. (*a*) $\overline{u^{+2}}$; (*b*) $\overline{v^{+2}}$; (*c*) $-\overline{u^+v^+}$. DNS (Kim *et al.* 1987): —; LDV (Wei & Willmarth 1989): - - -; PIV (Nishino & Kasagi 1989): – - –; Present: ○. Measured $\overline{v^{+2}}$ (Antonia *et al.* 1992): △; Corrected $\overline{v^{+2}}$ (present): □; calculated $-\overline{u^+v^+}$: – –.

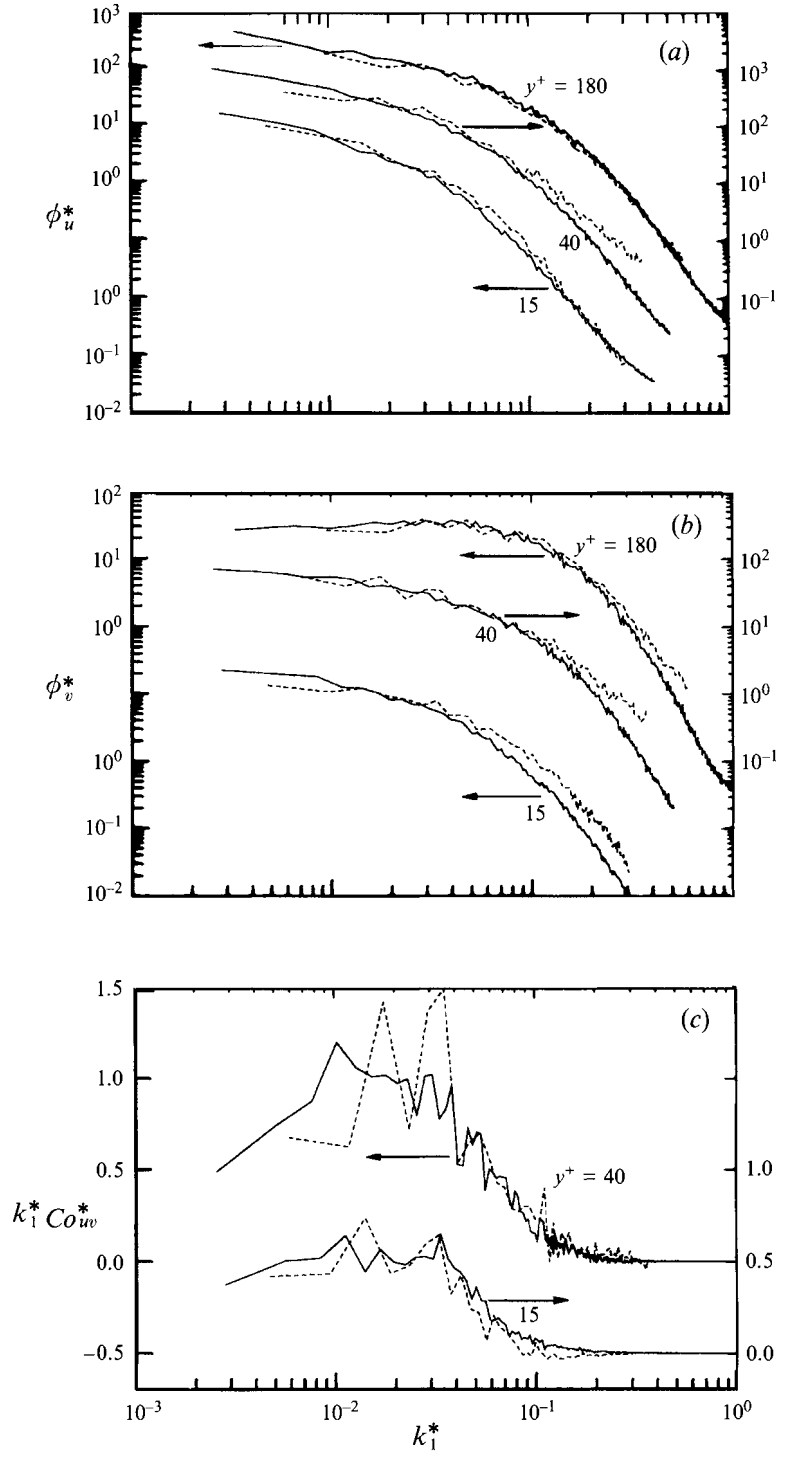

FIGURE 12. Comparison between measured and DNS spectra. (*a*) ϕ_u^*; (*b*) ϕ_v^*; (*c*) $k_1^* Co_{uv}^*$. Measured: —; DNS (Kim *et al.* 1987): - - -.

reflecting the adequacy of the choice of d. In the near-wall region (figure 11*b*), the present $\overline{v^2}$ measurements lie above the other three sets of data. Antonia *et al.*'s data are even higher as a result of too small a value of d^* (0.9 to 1.5).

After dividing the present data for $\overline{v^2}^m$ by r_v, the resulting distributions (figure 11*b*) are in quite good agreement with all the data, especially in the wall region. Unfortunately, the other data for $\overline{v^2}^m$ (Antonia *et al.* 1992) cannot be corrected in the same manner because of the type of error which occurred due to too small separation. This difficulty is similar to that encountered when derivative measurements are made with parallel hot wires with a separation $d^* \lesssim 2$ (Antonia *et al.* 1993; Zhu & Antonia 1992, 1993).

A check of the present data for $\overline{uv}$ can be obtained by comparing these data with values of $\overline{uv}$ calculated from the x-momentum equation

$$-\overline{uv} + \nu \frac{\mathrm{d}\overline{U}}{\mathrm{d}y} = U_\tau^2 \left(1 - \frac{y}{h}\right) \quad , \tag{7.1}$$

and the measured distribution of $\overline{U}$. The friction velocity U_τ was inferred from the measured pressure gradient and $\overline{U}$ was measured with a single hot wire. The calculated values of $-\overline{u^+v^+}$ are plotted in figure 11(*c*). The agreement between calculation and measurement is reasonable, allowing for the relatively large uncertainty in the present measurements in the wall region.

The present one-dimensional spectra $\phi_u(k_1)$, $\phi_v(k_1)$ and cospectra $Co_{uv}(k_1)$ (figure 12) are compared with the corresponding DNS data at $y^+ = 15$, 40 and 180 respectively. For the present data, the measured spectra and cospectra are used except for ϕ_u and ϕ_v at $y^+ = 180$; for the latter two, corrected spectra are used. The level of agreement between measured and DNS data is reasonable for the u spectra and the uv cospectra. The measured v spectra (figure 12*b*) tend to depart from the DNS data at high wavenumbers, this tendency being more emphasized near the wall.

The discrepancy between the measured and DNS spectra may be due to errors in both experiment and DNS data. For example, the x_1 resolution of the DNS data may be sufficiently poor ($\Delta x_1^+ = 11$, where Δx_1 is the grid size in the x_1 direction) to affect the dissipation part of the computed spectra. For the measured data, the finite wire separation attenuates the high wavenumber part of the spectra (figure 3*b*). At the channel centreline, the amount by which ϕ_v^* is underestimated is about 20% at $k_1^* = 1$. If wire length effects are taken into account, this amount could be as large as 40%. Even bigger attenuations are expected as the wall is approached. Other factors which may account for the discrepancy include the uses, in the measurements, of Taylor's hypothesis (when converting frequencies to wavenumbers) and of a low-pass filter cut-off frequency.

8. Conclusions

The effect of separation between the wires of an X-probe on the measurement of the Reynolds stresses has been examined by analysis and experiment. The spectral correction method of Wyngaard was modified to account for the effect of the tangential cooling of the wires and for any possible asymmetry of the probe. Experiments at the centreline of a turbulent channel flow, where isotropy is approximately satisfied, provide reasonable support for the modified analysis. The method becomes inadequate in the wall region where departures from isotropy are important. However, a knowledge of two-point velocity correlations allows the measured Reynolds stresses

to be corrected. Measurements in this region indicate that the effect of wire separation and effective angles is significant. Near the wall, the errors increase, especially for $\overline{v^2}$. Reasonable results for the Reynolds stresses and the corresponding spectra and cospectra can be obtained with a fixed separation probe when the separation is in the range 2–3 Kolmogorov length scales. This choice is justified by the agreement between the present results and the DNS, LDV and PIV data. Corrections are requested when larger separations are used. This is especially important if reliable data for $\overline{v^2}$ are to be obtained in the near-wall region.

The support of the Australian Research Council is gratefully acknowledged. We are also most grateful to Dr J. Kim for the DNS data.

REFERENCES

ANDREOPOULOS, J. 1983 Improvements of the performance of triple hot wire probes. *Rev. Sci. Instrum.* **54**, 733–740.

ANTONIA, R. A. 1991 Direct numerical simulations and hot wire experiments : A possible way ahead? *Monte Verita Colloquium on Turbulence, Ascona, Switzerland.*

ANTONIA, R. A., BROWNE, L. W. B. & CHAMBERS, A. J. 1984 On the spectrum of the transverse derivatives of the streamwise velocity in a turbulent flow. *Phys. Fluids* **27**, 2628.

ANTONIA, R. A., BROWNE, L. W. B. & SHAH, D. A. 1988*a* Characteristics of vorticity fluctuations in a turbulent wake. *J. Fluid Mech.* **189**, 349–365.

ANTONIA, R. A. & KIM, J. 1992 Isotropy of small scale turbulence. *CTR Summer School.*

ANTONIA, R. A. & KIM, J. 1993 Isotropy of the small-scales of turbulence at low Reynolds number. *J. Fluid Mech.* **251**, 219–238.

ANTONIA, R. A., SHAH, D. A. & BROWNE, L. W. B. 1988*b* Dissipation and vorticity spectra in a turbulent wake. *Phys. Fluids* **31**, 1805–1807.

ANTONIA, R. A., TEITEL, M., KIM, J. & BROWNE, L. W. B. 1992 Low-Reynolds-number effects in a fully developed turbulent channel flow. *J. Fluid Mech.* **236**, 579–605.

ANTONIA, R. A., ZHU, Y. & KIM, J. 1993 On the measurement of lateral velocity derivatives in turbulent flows. *Expts. Fluids* **15**, 65–69.

BATCHELOR, G. K. 1953 *The Theory of Homogeneous Turbulence.* Cambridge University Press.

BREMHORST, K. 1972 The effect of wire length and separation on X-array hot-wire anemometer measurements. *IEEE Trans. Instrum. Measurement* **IM-21**, 244–248.

BROWNE, L. W. B., ANTONIA, R. A. & SHAH, D. A. 1988 Selection of wires and wire spacing for X-wires. *Expts. Fluids* **6**, 286–288.

BRUUN, H. H. 1972 Hot wire data corrections in low and in high turbulence intensity flows. *J. Phys.* E: *Sci. Instrum.* **5**, 812–818.

BRUUN, H. H. & TROPEA, C. 1985 The calibration of inclined hot-wire probes. *J. Phys.* E: *Sci. Instrum.* **18**, 405–413.

CHAMPAGNE, F. H., SLEICHER, C. A. & WEHRMAN, O. H. 1967 Turbulence measurements with inclined hot-wires. *J. Fluid Mech.* **28**, 153–175.

HINZE, J. O. 1959 *Turbulence.* McGraw-Hill.

HISHIDA, M. & NAGANO, Y. 1988 Turbulence measurements with symmetrically bent V-shaped hot-wires. Part 1 : Principles of operation. *Trans. ASME* I: *J. Fluids Engng* **110**, 264–269.

HUNT, J. C. R., MOIN, P., MOSER, R. D. & SPALART, P. R. 1987 Self similarity of two point correlations in wall bounded turbulent flows. *Proc. Summer Program, Center for Turbulence Research, Stanford University/NASA-Ames*, pp. 25–36.

JÖRGENSEN, F. E. 1971 Directional sensitivity of wire and fiber-film probes. *DISA Information* **11**, 31–37.

KAWALL, J. G., SHOKR, M. & KEFFER, J. F. 1983 A digital technique for the simultaneous measurement of streamwise and lateral velocities in turbulent flows. *J. Fluid Mech.* **133**, 83–112.

KIM, J., MOIN, P. & MOSER, R. 1987 Turbulent statistics in fully developed channel flow at low Reynolds number. *J. Fluid Mech.* **177**, 133–166.

KURODA, A. 1990 Direct numerical simulation of Couette-Poiseuille flows. Doctor of Engineering Thesis, Department of Mechanical Engineering, University of Tokyo.

LOMAS, C. G. 1986 *Fundamentals of Hot Wire Anemometry.* Cambridge University Press.

NAKAYAMA, A. & WESTPHAL, R. V. 1986 The effects of sensor length and spacing on X-wire measurements in a boundary layer. *NASA Tech. Memo.* 88352.

NISHINO, K. & KASAGI, N. 1989 Turbulence statistics measurement in a two-dimensional channel flow using a three-dimensional particle tracking velocimeter. *Proc. Seventh Symposium on Turbulent Shear Flows, Stanford,* pp. 22.1.–22.1.6.

PAO, Y. H. 1965 Structure of turbulent velocity and scalar fields at large wavenumbers. *Phys. Fluids* **8**, 1063–1075.

PARK, S. R. & WALLACE, J. M. 1992 The influence of instantaneous velocity gradients on turbulence properties measured with multi-sensor hot-wire probes. *Thirteenth Symp. on Turbulence, University of Missouri-Rolla.*

PERRY, A. E. 1982 *Hot-Wire Anemometry.* Clarendon Press.

SHAH, D. A. 1988 Scaling of the "bursting" and "pulse" periods in wall bounded turbulent flows. PhD thesis, University of Newcastle, Australia.

SUZUKI, Y. & KASAGI, N. 1990 Evaluation of hot-wire measurements in turbulent wall shear flows using a direct numerical simulation data base. In *Engineering Turbulence Modelling and Experiments* (ed. W. Rodi & E. N. Ganić), pp. 361–370. Elsevier.

SWAMINATHAN, M. K., RANKIN, G. W. & SRIDHAR, K. 1986 Evaluation of the basic systems of equations for turbulence measurements using the Monte Carlo technique. *J. Fluid Mech.* **170**, 1–19.

TAGAWA, M., TSUJI, T. & NAGANO, Y. 1992 Evaluation of X-probe response to wire separation for wall turbulence measurements. *Expts. Fluids* **12**, 413–421.

TEITEL M. & ANTONIA, R. A. 1990 The interaction region in a turbulent duct flow. *Phys. Fluids* A **2**, 808–813.

TUTU, N. K. & CHEVRAY, R. 1975 Cross-wire anemometry in high intensity turbulence. *J. Fluid Mech.* **71**, 785–800.

VUKOSLAVČEVIĆ, P. & WALLACE, J. M. 1981 Influence of velocity gradients on measurements of velocity and streamwise velocity with hot-wire X-array Probes. *Rev. Sci. Instrum.* **52**, 869–879.

WEI, T. & WILLMARTH, W. W. 1989 Reynolds-number effects on the structure of a turbulent channel flow. *J. Fluid Mech.* **204**, 57–95.

WESTPHAL, R. V. 1990 Near-wall measurement errors for hot-wire probes with finite spatial resolution. *Proc. ASME Symp., Toronto,* pp. 1–8.

WYNGAARD, J. C. 1968 Measurement of small-scale turbulence structure with hot wires. *J. Phys.* E: *Sci. Instrum.* **1**, 1105–1108.

ZHU, Y. & ANTONIA, R. A. 1992 The measurement of $\partial u/\partial y$ in the wall region of a turbulent channel flow. *Proc. Eleventh Australasian Fluid Mechanics Conf., Hobart, Australia,* pp. 695–698.

ZHU, Y. & ANTONIA, R. A 1993 Temperature dissipation measurements in a fully developed turbulent channel flow. *Expts. Fluids* **15**, 191–199.

ZHU, Y., ANTONIA, R. A. & KIM, J. 1993 Velocity and temperature derivative measurements in the near-wall region of a turbulent duct flow. In *Near-Wall Turbulent Flows* (ed. R. M. C. So, C. G. Speziale & B. E. Launder), pp. 549–561. Elsevier.